Tackling Modelling Error in the Application of Electrical Impedance Tomography to the Head

Tackling Modelling Error in the Application of Electrical Impedance Tomography to the Head

Taweechai Ouypornkochagorn, Hugh McCann, and Nick Polydorides

Abstract— **In the head application of Electrical Impedance Tomography (EIT), reconstruction of voltage measurements for a conductivity distribution image using an ordinary method, the absolute imaging approach, is impossible due to the traditional ignorance of modelling error. The modelling error comes from the inaccuracy of geometry and structure, which are unable to be known accurately in practice, and are usually large in head application of EIT. Difference imaging is an alternative approach which is able to reduce the size of this error, but it introduces other kinds of error. In this work, we demonstrate that in situations like head EIT, the nonlinear difference imaging approach can reconstruct difference conductivity effectively: the reduced modelling error and the new errors arising are able to be ignored, because they are much smaller than the original modelling error. The magnitude of conductivity change in the head-like situation is also investigated, and a selection scheme for the initial guess in the reconstruction process is also proposed.**

I. Introduction

Electrical Impedance Tomography (EIT) is a soft-field modality, which is able to reconstruct the spatial distribution of conductivity inside a body of interest as an image. However, EIT is very vulnerable to noise and error. In the case of *in vivo* EIT, particularly in application to the head, noise such as measurement or instrument noise may be minimized to a satisfactory level, but this is not possible in the case of the modelling error [1]. The various sources of modelling error include inaccuracy of the tissue geometries and conductivities, and of the position and contact impedance of electrodes. In turn, these cause the prediction model (the forward model) to yield significant mismatches with real measurements [2]. However, these sources of modeling error are difficult or impossible to correct. As a result, modelling error is usually ignored in these cases. In a homogeneous situation e.g. in [3], reconstruction using the standard approach – absolute imaging - is possible due to the small size of the error. However, in the case of head EIT this is not possible - the modelling error is too large. Additionally, the sensitivity of the voltage measurements to changes in the conductivity of the brain is extremely low due to the presence of the skull and the cerebrospinal fluid (CSF). This condition makes this problem severely ill-posed and more sensitive to the modelling error.

The difference imaging approach is an alternative to directly reconstructing the difference of conductivity between two recording times [3]. The modelling error is reduced by the subtraction between two sets of measurement data. However this still suits better the situation where the conductivity of the referent state is known. In the case of head EIT, the conductivity of the referent state, i.e. the conductivity of all head tissues, is impossible to know accurately. The reported values of the tissue conductivities are usually selected as the reference instead. Therefore some small error is usually introduced [4].

In this paper, the difference imaging approach was investigated when it was used in situations where the geometry and structure of the subject were modelled inaccurately. The conventional formula of this approach was transformed into the conventional form of the absolute imaging approach, and then nonlinear reconstruction algorithms were used for reconstruction. The expectation was that this approach is more robust to the ignorance of the modelling error term than the absolute imaging approach. A selection scheme for the initial guess of the conductivity distribution in the reconstruction process is also proposed.

II. Errors in Difference Imaging Approach

For the recording index i of a measurement time series, the measurement model is determined by the discretized function U of the conductivity σ_i in the addition of the modelling error function ε and the measurement error e_m (1). However, the modelling error is practically unknown, and it is usually ignored [3]. Therefore, the estimation $\hat{\sigma}_i$ can be determined by the absolute imaging approach with the regularization function R and the regularization parameter λ as in (2).

$$V_i = U(\sigma_i) + \varepsilon(\sigma_i) + e_m; \quad e_m \sim N(0, \Gamma_e) \tag{1}$$

$$\hat{\sigma}_i = \arg\min_{\sigma} \left\{ \|V_i - U(\sigma_i)\|^2 + \lambda \|R(\sigma_i)\|^2 \right\} \tag{2}$$

When the change in conductivity is small, the modelling error is assumed to be only slightly changed, and its effect can be reduced by the subtraction between two consecutive measurements V as in (3), and the difference voltage vector δV can then be approximated in the form of a linear difference imaging approach (4) where e_L is the linearization error. Unfortunately the exact σ_{i-1} of the reference state (or the previous state), used to compute the Jacobian $U'(\sigma_{i-1})$ (the sensitivity) cannot be known in head EIT. The closest known values are the conductivities obtained from literature, denoted by σ_{init}.

$$V_i - V_{i-1} = U(\sigma_i) - U(\sigma_{i-1}) + \delta\varepsilon + \delta e_m = \delta V_{(i,i-1)} \tag{3}$$

$$\delta V_{(i,i-1)} = U'(\sigma_{i-1})(\sigma_i - \sigma_{i-1}) + e_L + \delta\varepsilon + \delta e_m \text{ , where} \tag{4}$$

$$U'(\sigma_{i-1}) = \frac{\partial U(\sigma_{i-1})}{\partial \sigma}, \ \delta e_m \sim N(0, \Gamma_e + \Gamma_e)$$

In this work, we hypothesize that the Jacobian $U'(\sigma_{init})$ has similar characteristics to $U'(\sigma_{i-1})$. The conductivity difference

Taweechai Ouypornkochagorn, Hugh McCann, and Nick Polydorides are with the School of Engineering at the University of Edinburgh, Edinburgh, EH9 3JL, UK; e-mail: t.ouypornkochagorn@sms@ed.ac.uk).

image can be computed from the difference between σ_{init} and the new replacement unknown $\tilde{\sigma}_i$ instead (5). Then when (5) is approximated back to the nonlinear function form (6), this estimation introduces the error e_J, named the Jacobian estimation error (7). Substitution of (7) into (4) then yields (8). Last but not least, (8) can be written in the conventional form as in (9) - the measurement V in (1) becomes $\tilde{V}$, and the error term becomes e_δ, that is the sum of e_L, e_J, and $\delta\varepsilon$, representing the overall difference imaging error. Similar to the absolute imaging approach, due to the unknown value of e_δ, it is then ignored and the estimation of $\tilde{\sigma}_i$ can be found by (10). At this point, any nonlinear iterative reconstruction algorithm can be used. The key issue examined here is the impact of the ignorance of ε in the absolute imaging approach and that of e_δ in the difference imaging approach.

$$U'(\sigma_{i-1})(\sigma_i - \sigma_{i-1}) \approx U'(\sigma_{init})(\tilde{\sigma}_i - \sigma_{init}) \quad (5)$$

$$\approx U(\tilde{\sigma}_i) - U(\sigma_{init}) \quad (6)$$

$$U'(\sigma_{i-1})(\sigma_i - \sigma_{i-1}) = U(\tilde{\sigma}_i) - U(\sigma_{init}) + e_J \quad (7)$$

$$\delta V_{(i,i-1)} = U(\tilde{\sigma}_i) - U(\sigma_{init}) + e_J + e_L + \delta\varepsilon + \delta e_m \quad (8)$$

$$\tilde{V}_{(i,i-1)}(\sigma_{init}) = U(\tilde{\sigma}_i) + e_\delta + \delta e_m, \text{ where} \quad (9)$$

$$\tilde{V}_{(i,i-1)}(\sigma_{init}) = U(\sigma_{init}) + \delta V_{(i,i-1)} \text{ and } e_\delta = e_J + e_L + \delta\varepsilon$$

$$\tilde{\sigma}_i = \arg\min_{\tilde{\sigma}} \left\{ \left\| \tilde{V}_{(i,i-1)}(\sigma_{init}) - U(\tilde{\sigma}_i) \right\|^2 + \lambda \left\| R(\tilde{\sigma}_i) \right\|^2 \right\} \quad (10)$$

Furthermore, in order to estimate the change for the next image ($\tilde{\sigma}_{i+1}$), the traditional way is to replace σ_{init} with the $\tilde{\sigma}$ of the previous image in (10). However, $\tilde{\sigma}$ in some particular images might be very inaccurate due to high measurement noise, meaning that $U'(\sigma_i)$ might be very different to $U'(\tilde{\sigma}_i)$. This phenomenon ruins all the images after i. Here, we propose to keep using σ_{init} for the whole image sequence.

III. Methods and Materials

A. Simulation

A simple head EIT situation was simulated. Two circular head-like layerwise models of 170mm diameter were created to represent the layers of the scalp, the skull, the CSF, and the brain. The models are finite element models (FEM): the first model is finer and used as the forward model (with 10,816 elements) (Fig. 1a), and another is used as the inverse model (with 9,216 elements) (Fig. 1b). The thickness and the conductivity of each layer were set as in Table 1 – the significant differences between the models are in the scalp and skull layers. Three test inclusions were simulated as in Fig. 1c. Two test schemes were designed: large conductivity change and small conductivity change (Table 2). The simulated current is 1mA$_{pk-pk}$ operated in diametric current patterns on a 16-electrode setting, and 208 nearest-neighbor measurements are obtained. The signal-to-noise ratio of the simulated measurements is set to 50dB. A non-linear regularized Gauss-Newton algorithm was used to reconstruct the images of difference conductivity (i.e. with/without the inclusions) with 10 iterations. The difference images reconstructed by the absolute imaging approach and the difference imaging approach explained in the previous section were compared by using λ of 0.1, for the absolute imaging approach, and 0.001, for the difference imaging approach.

TABLE I. Thicknesses and Conductivities of the Models

Layer[a]	Forward Model		Inverse Model	
	Thickness (mm)	*Conductivity (S/m)*	*Thickness (mm)*	*Conductivity (S/m)*
Scalp	7	0.58 [5]	8.87	0.4348 [6]
Skull	6	0.008 [5]	3.54	0.0154 [7]
CSF	7	1.802 [8]	7.08	1.802 [8]
Brain	radius = 65	0.2849 [9]	radius=65.5	0.2849 [9]

a. Order from the outermost layer to the innermost layer

TABLE II. The Simulation Schemes

Testing Object	Location	Scheme1: Small change Conductivity (S/m)	Scheme2: Large change Conductivity (S/m)
Inclusion 1	Scalp	0.551 (-5%, -0.03)	0.493 (-15%, -0.09)
Inclusion 2	CSF	1.748 (-3%, -0.05)	1.623 (-10%, -0.18)
Inclusion 3	Brain	0.646 (+127%,+0.36)	0.646 (+127%,+0.36)

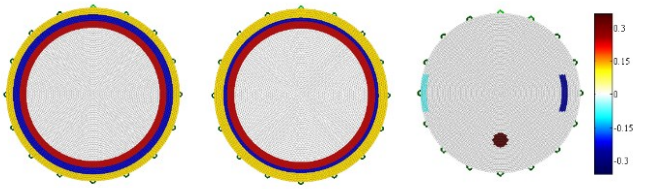

(a) (b) (c)

Figure 1. (a) Forward model, (b) Inverse model, and (c) the location and size of the test inclusions (see Table II).

B. Phantom Experiments

Two experiments were performed on a head-shape tank (Fig. 2a). The distance between the nasion and the inion, and between the left-right preauricular, following the standard EEG 10-20 system, are both 360 mm. In the first experiment, the tank was filled with 2.7 S/m-saline; meanwhile in the second experiment, a honeydew melon peel was put inside the tank filled with the same concentration of saline (Fig. 2b). The peel was approximately 10mm in thickness, and it was naturally dried for a week in order to minimize the moisture content. The major radius and the minor radius of the peel are 85 mm and 70 mm respectively. A FEM head-shape model was created from a Magnetic Resonance image having 93,687 elements (Fig. 2c). However, the two distances (nasion-inion, left-right preauricular) of the model were both 380 mm. The electrode geometry and the melon peel geometry were also included in the model. The test inclusion is a carrot of 13.5 mm-radius and 28 mm-length. The carrot was dipped with its full length into the center of the tank and moved to the left then the right for the first experiment. It was then dipped into the center of the melon peel and removed for the second experiment. The experiments were carried out with the fEITER system [10] with 100 frames per second recording speed. An electrode array of 32 electrodes was attached, and 546 measurements were taken for each record. The injected current was 1 mA$_{pk-pk}$ at 10 kHz. In order to minimize measurement noise, the measurements were averaged over a 0.5 second-period (50 records).

The absolute imaging approach and difference imaging approach were investigated here. In addition, the initial selection schemes: using the $\tilde{\sigma}$ of the previous image, and maintaining the use of σ_{init}, were compared in the second experiment. The reconstruction algorithm used is the regularized General Minimal Residual (GMRes) [11] with 10

iterations, with λ set to $1x10^{-3}$, for the absolute imaging approach, and $1x10^{-7}$, for the difference imaging approach. Moreover, due to the unknown conductivity of the melon peel, the conductivity of the peel was investigated by following the methodology in [5] and imposing positivity [12] by using a regularization parameter of $1x10^{-3}$ and a starting guess conductivity of 0.1 S/m. However, the peel conductivity was kept unchanged in the reconstruction process of the second experiment, since the conductivity of the peel is not changed and the sensitivity of the algorithm to the peel is extremely high.

IV. Results

A. Simulation

The reconstruction images of the two approaches are shown in Fig. 3. Obviously, the difference imaging approach is able to detect the inclusions in both schemes. Meanwhile, the reconstruction with the absolute imaging approach is unable to detect the inclusion even in the small change scheme. However, the magnitude of conductivity change at the inclusion region with the difference imaging approach is unable to reflect the true change – it is lower, and it tends to be much lower in the inner layers. Furthermore in the large change scheme using the difference imaging approach (Fig. 3d), the amplitude of the ringing effect on the outermost layer (represented by the dark red color) is very high, and also is higher than the amplitude of the inclusion in the brain region (represented by the lighter red color).

(a) (b) (c)

Figure 2. (a) Head-shape tank, (b) Honeydew melon peel put inside (in the second experiment) and the test inclusion, a carrot, (c) the inverse tank model.

TABLE III. The Size of Errors

Error	Scheme1: Small change	Scheme2: Large change
$\|\varepsilon + e_m\|$	0.7176	0.7224
$\|e_\delta + \delta e_m\|$	0.0066	0.0231

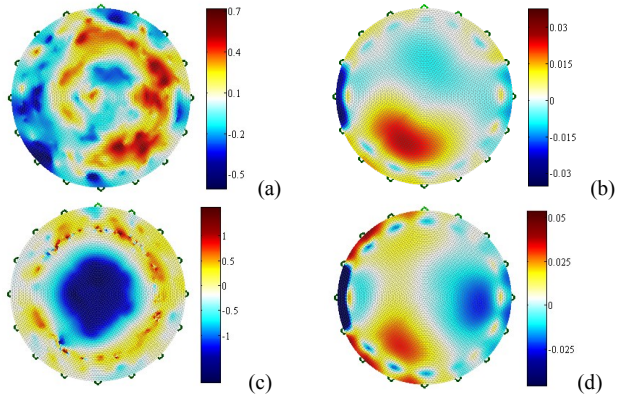

Figure 3. Reconstruction images of the small change scheme (top row) and the large change scheme (bottom row): the absolute imaging approach (a,c) and the difference imaging approach (b,d).

The true sizes of the errors in (1) and (9) are computed and shown in Table 3. Obviously, the size of the ignored modelling error, computed from (1), is very much higher than the size of the ignored difference imaging error, computed from (9), by about 30-110 times. It can be also noticed that the size of the latter error is increased when the size of change increases and these increments are correlated: the ~3 time-conductivity increment leads to a 3.5 time-error increment.

B. Phantom Experiments

The four chosen reconstruction images of the first experiment (no peel) are shown in Fig. 4. The movement of the dipped object is able to be seen only in the images obtained from the difference imaging approach; however some of the incorrect artefacts remain in the late images. In the absolute imaging approach, the color of the changing artefacts is meaningless and the change was significantly retained even though the object has been removed. Therefore, these changing artefacts might be the reconstruction error due to the modelling error rather than the reconstructed inclusion.

Regarding the second experiment (with peel), the conductivity of the peel was evaluated first (Fig. 5), and the result shows that the best estimation value is 0.0016 S/m, and it was used as the initial guess for the reconstruction. The chosen images are shown in Fig. 6. The outcome is consistent with the first experiment – the dipping is able to be effectively detected in the difference imaging approach (Fig. 6 - bottom row), but it is not detectable in the absolute imaging approach (Fig. 6 - top row). However, the conductivity change of the detected inclusion is much lower than those observed in the first experiment.

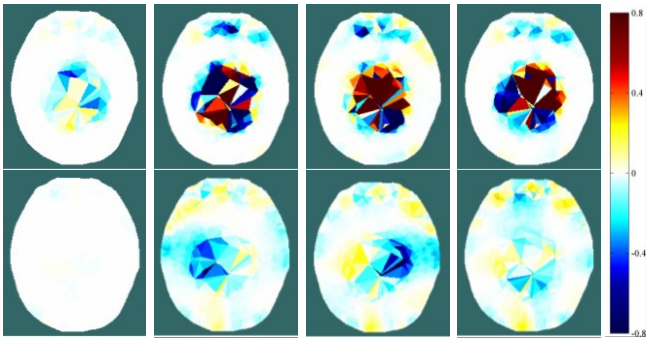

Figure 4. Reconstruction images of the first experiment (no peel) from the beginning of dipping (no carrot) – the leftmost column - to full inclusion of the carrot on the left, then on the right, and finally the carrot was removed – the rightmost column: the absolute imaging approach (top row) and the difference imaging approach (bottom row).

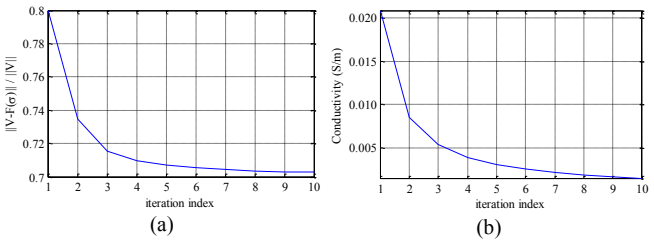

Figure 5. The estimation of the melon peel conductivity: (a) the data misfit, (b) the estimation conductivity

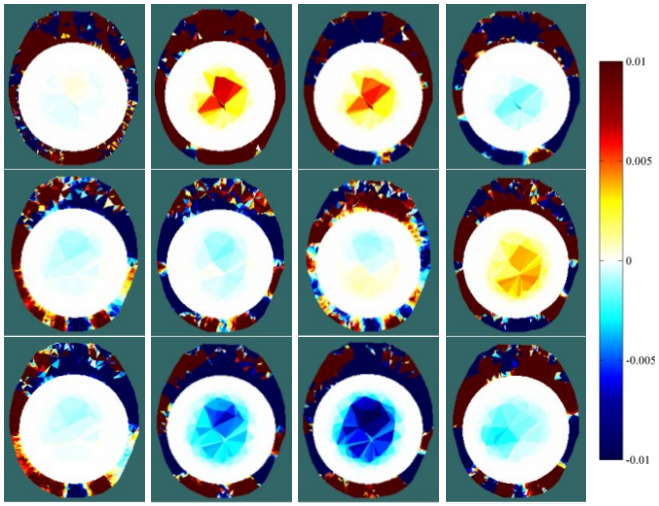

Figure 6. Reconstruction images of the second experiment (with the peel) from the begin to the end of dipping: the absolute imaging approach (top row), and the difference imaging approach: using the previous image estimate $\tilde{\sigma}$ (middle row), and with retained use of σ_{init} (bottom row).

The selection scheme of the initial guess impacts the image accuracy. Selecting the previous estimate $\tilde{\sigma}$ as the initial value yields inaccurate images (the two last images of Fig. 6 – middle row). We remark that the incorrect electrode artefacts with high amplitude at the boundary are clearly seen for both approaches. This is a typical behavior of head EIT due to imprecise electrode setting [2].

V. Discussion

It is obvious that the modeling error, which is normally ignored or determined as zero mean value in the absolute imaging approach, is vital. Unfortunately, in applications where the geometry and structure are inaccurate, such as head EIT, the modelling error is impossible to avoid due to lack of sufficient knowledge. This is the primary reason of the reconstruction failure in the absolute imaging approach as seen in both the simulation and the experiments. The difference imaging approach is able to reduce the size of this error, but it introduces a new kind of error which also has to be ignored due to inability to measure. The difference imaging approach, however, achieves reasonable reconstructions in all situations reported here, because the size of the ignored error is much lower than the ignored modelling error.

The unrealistic magnitude of the reconstructed change in conductivity of the inclusions and the amplitude of unwanted artefacts are an interesting behavior in head EIT. According to the simulation, the amplitude of the inclusion in the scalp layer is presumably accurate, but the amplitude of the inclusions inside the skull layer are substantially lower than the true amplitude, in particular in the brain region. The phenomenon is caused by the very low sensitivity of those regions. Therefore, the true amplitude of conductivity change is unable to be imaged in head EIT. This behavior perfectly matches the difference imaging approach, because we must assume some known conductivities as the conductivity of the referent state and this then leads to inaccurate amplitude of the estimation. However, one of the greatest concerns is the high amplitude-unwanted artefacts on the scalp layer. Even though it is very typical to have these artefacts due to the presence of noise and error, their amplitude is generally higher than the amplitude of the reconstructed inclusions situated inside the skull layer. It can also be noticed from the simulation that if the size of the changes is high, it will produce higher amplitude unwanted artefacts in the scalp layer. Therefore, the system which has higher recording speed is advantageous relative to the slower one, because the change between two consecutive records is likely to be smaller.

The size of regularization parameter is another benefit for the difference imaging approach. Due to the substantial reduction of the error, the regularization does not need to be high. A chosen value from a record tends to be reusable for the whole sequence of records. Unlike the absolute imaging approach, where many values (even though they are pretty high) might yield a singular matrix, and are unable to be solved; it is then very difficult to find a value which is able to be reused for the other records.

The selection of initial value of conductivity is a critical issue for reconstructing a long recording. The conventional methodology of using the estimate of the previous record is vulnerable to short-term high-noise on some records or inaccuracy of estimation. This leads to a wrong estimation beginning from the high-noise record to the last record. Therefore in the head EIT, using the same initial value for the whole sequence of records is more robust in practice.

References

[1] W. R. B. Lionheart, "EIT reconstruction algorithms: pitfalls, challenges and recent developments," *Physiol. Meas.,* vol. 25, 2004.

[2] A. Boyle and A. Adler. "The impact of electrode area, contact impedance and boundary shape on EIT images," *Physiol. Meas*. vol. 32, pp. 745-754, 2011.

[3] D. Liu, V. Kolehmainen, S. Siltanen, and A. Seppänen, "A nonlinear approach to difference imaging in EIT; assessment of the robustness in the presence of modelling errors," *Inverse Problems*, vol. 31, 2015.

[4] A. Adler, "Variability in EIT Images of Lungs: Effect of Image Reconstruction Reference," *The 12th Int. Conf. Electrical Bio-impedance and the EIT*, Poznan, Poland, 2004.

[5] T. Ouypornkochagorn, N. Polydorides, and H. McCann, "In Vivo Estimation of the Scalp and Skull Conductivity," *The 15th Int. Conf. Biomedical Application of EIT*, 2014.

[6] H. C. Burger and J. B. Milaan, "Measurements of the specific Resistance of the human Body to direct Current," *Acta Medica Scandinavica*, CXIV(VI), 1943.

[7] T. F. Oostendorp and J. Delbeke, "The conductivity of the human skull in vivo and in vitro," *The 21st Annual Conf. and the 1999 Annual Fall Meeting of the Biomedical Engineering Soc*, 1999.

[8] S. B. Baumann, D. R. Wozny, S. K. Kelly, and F. M. Meno, "The Electrical Conductivity of Human Cerebrospinal Fluid at Body Temperature," *IEEE Trans. biomedical engineering*, vol. 44(3), 1997.

[9] J. A. Latikkal, J. A. Hyttinen, T. A. Kuume, H. J. Eskola, and J. A. Malmivuo, "The conductivity of brain tissues: comparison of results in vivo and in vitro measurements," *The 23rd Annual Inter. Conf. of the IEEE Engineering in Medicine and Biology Society*, 2001.

[10] H. McCann, S. T. Ahsan, J. L.Davidson, R. L. Robinson, P. Wright, and C. J. D. Pomfrett, "A portable instrument for high-speed brain function imaging: fEITER," *The 33rd Annual Inter. Conf. of the IEEE EMBS*, Massachusetts, USA, 2011.

[11] L. Horesh, M. Schweiger, S. R. Arridge, and D. S. Holder, "Large-Scale Non-Linear 3D Reconstruction Algorithms for Electrical Impedance Tomography of the Human Head," *World Congress on Medical Physics and Biomedical Engineering*, 2006.

[12] N. Polydorides, T. Ouypornkochagorn., and H. McCann, "Inequality Constrained EIT Modelling and Inversion," *The 15th Inter. Conf. Biomedical Application of EIT*, 2014.